

A Discussion on Nonlinear Analysis of RCFT Columns

○Alifujiang Xiamuxi*, Akira Hasegawa**

*Student member, PhD Student, Dept. of Environmental and Civil Eng., Hachinohe Institute of Technology
(College of Architectural and Civil Engineering, Xinjiang University, Urumqi 830008, China)

**Regular member, Professor, Dept. of Environmental and Civil Eng., Hachinohe Institute of Technology

1. INTRODUCTION

The brittle-failure is concerned when it is considered to construct large-scaled structures with concrete filled tubular steel (CFT) structures, and then, reinforced concrete filled tubular steel (RCFT) structures which are aimed at improving the brittle-failure resistibility of CFT structures by inserting the reinforcements is developed and studied in the terms of practical utilization. Fig.1 shows the model of CFT and RCFT.

Some research results until now proved that the performance of RCFT differed from that of CFT because of the existence of reinforcement. These are maybe mainly due to enhancement in performance of the core concrete because of the confinement pressure provided by both steel tube and reinforcement. Thus, the analytical methods used in nonlinear analysis of CFT, cannot be completely applied to RCFT structures.

The main purpose of this investigation is to establish a proper nonlinear analysis method for RCFT columns under axial compression. To achieve this goal, appropriate nonlinear constitutive material models for the confined concrete, steel tube, reinforcements are proposed. Then, the nonlinear finite element method (FEM) program ADINA is employed to perform numerical simulations of RCFT columns subjected to axial compressive forces. The proposed material constitutive models as well as the predicted ultimate strengths of RCFT columns are verified against experimental data. Finally, the influence of the concrete confining pressure is studied and discussed.

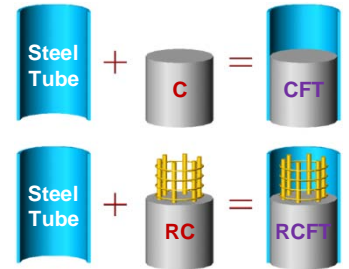


Fig.1 Model of CFT and RCFT

2. FEM MODELING

Concrete: the concrete of RCFT is in a multiaxial stress condition due to the confinement pressure by both steel tube and reinforcements. The key point on modeling the concrete is focuses on how to determine the multiaxial stress-strain relationship. Generally, the multiaxial stress-strain relations can be derived from uniaxial stress-strain relationship, shown as Fig.2.

It is known that the increase in strength of confined concrete is a result of the combination of lateral pressure and axial compression. In RCFT, the lateral pressure is provided by both steel tube and reinforcement. Whatever the confinement pressure, the strength of confined concrete may be expressed as the multiple of the strength of unconfined concrete and the strength increase due to the confining stresses:

$$\sigma_c = k_c \sigma_{co} \quad (1)$$

where k_c represents the strength increase coefficient due to confinement effect of steel tube and reinforcement to core concrete.

The other parameters to define multiaxial stress-strain relationship may be presented by the same concept as following expressions:

$$\sigma_u = k_3 \sigma_{uo}; \quad \varepsilon_c = (C_1 k_c^2 + C_2 k_c) \varepsilon_{co} \quad (2)$$

Based on the other study results, parameter ε_u can be ranged in:

$$1.2\varepsilon_c \leq \varepsilon_u \leq 11\varepsilon_c \quad (3)$$

Thus, the constants σ_c , σ_u , ε_c , ε_u can be employed instead of the uniaxial variables in order to establish, using the equations for uniaxial law by Saenz, the multiaxial stress-strain law (see Fig.2). A Kupfer model is employed as failure criterion.

Steel tube and reinforcement: the response of the steel tube and reinforcement is modeled by an elastic-perfectly-plastic theory with associated flow rule. A von Mises yield criterion is employed as failure criterion and a bilinear stress-strain relationship without strain hardening is employed as constitutive law.

Contact modeling: Pre-calculations on RCFT columns were performed with and without friction between steel tube and concrete, and the results showed that there were no obvious differences between the analysis results of the frictional and frictionless treatments, only the frictional treatment showed more time-consuming and convergence problem. Therefore, in this study, a constraint-function model with frictionless contact built in ADINA is employed.

3. IMPLEMENTATION PROGRAM

According to JSCE code the equation for load-sharing ratio of CFT takes the form as $\gamma_c = N_{so}/(N_{so} + N_{co})$. Taking the axial reinforcement into account, load-sharing ratio of RCFT may be expressed as:

$$\gamma_s = N_{so}/(N_{so} + N_{ro} + N_{co}) \quad (4)$$

As described in previous section, σ_c , σ_u , ε_c and ε_u should be provided in order to completely define the multiaxial stress-strain relation for core concrete. These parameters apparently depend on the γ_s . Consequently, their appropriate values can be

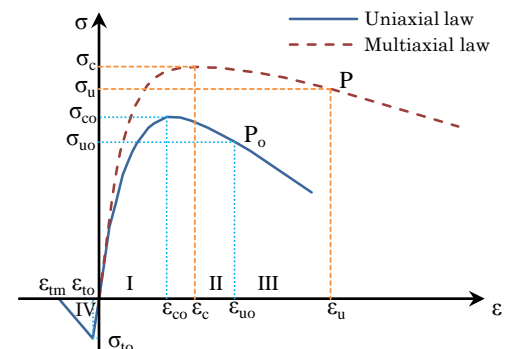


Fig.2 Constitutive law for concrete

Keywords: RCFT; CFT; numerical analysis; confinement effect

Contact: Ohbiraki 88-1, Hachinohe 031-8501, Japan E-mail: d10301@hi-tech.ac.jp TEL: 0178-25-8075

Table 1 Experimental parameters and results of numerical analysis

Labels	Experimental parameters							Results of numerical analysis									
	f_{sy} (MPa)	f_{ry} (MPa)	σ_{co} (MPa)	t (mm)	d_s (mm)	ρ (%)	γ_s	σ_c (MPa)	k_c	k_3	Bearing capacity N_u (kN)			Displacement δ (mm)			R^2
											N_u^T	N_u^A	N_{err} (%)	δ^T	δ^A	δ_{err} (%)	
RF70	285.0	235.0	19.2	6.0	6	1.3	0.70	43.18	2.25	1.00	1509.5	1511.3	-0.12	23.08	23.40	-1.40	0.991
RF64	296.0	235.0	19.2	4.5	6	1.2	0.64	42.56	2.22	1.00	1374.1	1359.6	1.06	12.13	12.30	-1.38	0.984
RF55	299.0	235.0	19.2	3.2	6	1.2	0.55	32.03	1.67	1.00	1052.6	1031.8	1.97	11.48	11.70	-1.93	0.969
RF48	314.0	352.0	27.1	3.2	6	1.2	0.48	41.54	1.53	1.00	1232.8	1247.4	-1.18	7.77	8.10	-4.23	0.926
RF31	327.3	295.0	44.3	2.3	6	1.1	0.31	54.58	1.23	0.97	1313.2	1309.0	0.32	3.84	3.90	-1.57	0.985
RF21	304.0	295.0	33.6	1.2	6	1.1	0.21	36.97	1.10	0.78	870.5	874.4	-0.45	2.70	2.70	-0.14	0.955
RF19	323.0	355.0	40.8	1.2	6	1.1	0.19	58.84	1.44	0.83	1263.7	1273.3	-0.76	2.62	2.70	-2.98	0.986
RF18	323.0	355.0	40.8	1.2	10	2.5	0.18	48.69	1.19	0.50	1162.4	1154.9	0.65	2.76	2.80	-1.56	0.989
RF16	323.0	355.0	40.8	1.2	13	4.4	0.16	54.59	1.33	0.39	1376.5	1364.7	0.86	2.51	2.70	-7.63	0.940

determined by matching the numerical results with experimental results via parametric study.

The experimental data with varying γ_s , collected by Hasegawa laboratory are used to verify and calibrate the numerical results, as shown in Table 1.

For each column, the calibration process is: 1) Start the calculation with σ_{co} , σ_{uo} , ε_{co} and ε_{uo} ; 2) Perform calculations by adjusting σ_c until the differences N_{err} of experimental bearing capacity N_u^T against analytical bearing capacity N_u^A satisfies $N_{err} \leq 3.0\%$; 3) At the starting of this stage, a k_c is already achieved. Continue calculations by using Eq.(2) and Eq.(3) and

adjusting σ_u and ε_u until the differences δ_{err} of experimental displacement δ^T (corresponding to N_u^T) against analytical displacement δ^A (corresponding to N_u^A) satisfies $\delta_{err} \leq 10.0\%$, and the correlation coefficient R^2 between experimental and analytical load-displacement curve satisfies $R^2 \geq 0.9$; 4) Stop calculations if N_{err} , δ_{err} and R^2 satisfied $N_{err} \leq 3.0\%$, $\delta_{err} \leq 10.0\%$, and $R^2 \geq 0.9$, respectively.

4. RESULTS AND DISCUSSION

The results of numerical analysis for the columns are given in Table 1. As a representative, the curve of axial force versus axial displacement is plotted against the experimental data for column RF48 in Fig.3. Generally, the numerical results show very good agreement with the experimental data.

It can be observed that the confinement effect k_c is not proportional to the load-sharing ratio γ_s . It is affected by the thickness of steel tube, the ratio of axial reinforcement and the strength of concrete.

When the γ_s is big (i.e., the steel tube thickness is relatively thick), the steel tubes provide strong lateral support to the concrete core, and brings in bigger values for k_c . On the other hand, when the γ_s is small (i.e., the steel tube thickness is relatively thin), the steel tubes provide weak lateral support to the concrete core, as a result, the k_c usually has relatively small values (say 1.10 for RF21 column), but a combination with high strength concrete gives the column bigger k_c (say 1.442 for RF19 column), meanwhile, the increase of axial reinforcement ratio also helps in increase of k_c (say 1.193 and 1.338 for RF18 and RF16 column, respectively). In addition, the behaviors of RCFT columns (e.g., RF16, RF18, RF18 and RF21 columns) are highly influenced by the parameter k_3 of concrete, it also can be noticed that increase in ratio of axial reinforcement and/or strength of concrete never bring increase in k_3 but k_c . Based on the results of k_c from numerical analysis, an empirical equation may be proposed as:

$$k_c = 5.71\gamma_s^2 - 2.96\gamma_s + 1.62 \quad (5)$$

where the value of γ_s should be in the range of $0.1 \leq \gamma_s \leq 0.9$ for RCFT columns.

The fitted curve is shown in Fig.4, and the correlation coefficient between observed data and fitted curve is $R^2=0.929$, means that the fitted curve matches the analytical results of k_c well.

5. CONCLUSIONS

The FEM model introduced in this paper, in cooperation with ADINA software, can be applied to nonlinear analysis of RCFT columns with reliable results.

The concrete in RCFT is in a 3-dimensional stress state, and its strength is increased compared with uniaxial stress state due to the confinement pressure around it provided by steel tube and reinforcement. As a result, a coefficient k_c called confined effect and concerned with load-sharing ratio γ_s of RCFT columns is introduced to evaluate the effect of that confinement pressure.

In this paper, the RCFT columns only under the axial compression was studied, and the FEM analysis of RCFT columns subjected to an axial compression and bending moment in combination are needed to be studied to further clarify mechanical properties of RCFT columns.

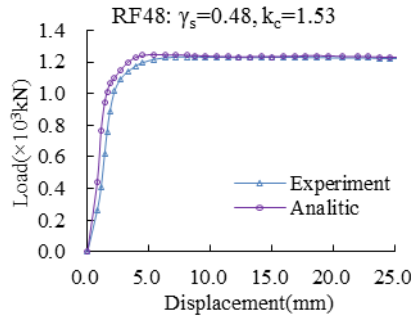
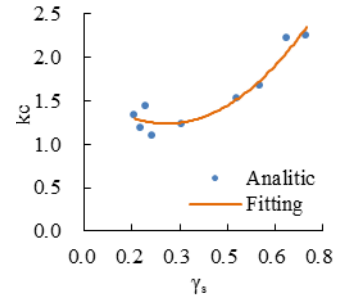


Fig.3 Load-displacement curve

Fig.4 k_c versus γ_s